The Journal of Experimental Biology 210, 4437-4447
Published by The Company of Biologists 2007
doi:10.1242/jeb.010322

Control of neuronal firing by dynamic parallel fiber feedback: implications for electrosensory reafference suppression

John E. Lewis[1,*], Benjamin Lindner[2], Benoit Laliberté[1] and Sally Groothuis[1]

[1]*Department of Biology and Center for Neural Dynamics, University of Ottawa, 30 Marie Curie, Ottawa, Ontario, K1N 6N5, Canada and* [2]*Max-Planck-Institute for the Physics of Complex Systems, Nöthnitzer Strasse 38, 01187 Dresden, Germany*

*Author for correspondence (e-mail: john.lewis@uottawa.ca)

Accepted 1 October 2007

Summary

The cancellation of self-generated components of sensory inputs is a key function of sensory feedback pathways. In many systems, cerebellar parallel fiber feedback mediates this cancellation through anti-Hebbian plasticity, resulting in the generation of a negative image of the reafferent inputs. Parallel fiber feedback involves direct excitation and disynaptic inhibition as well as synaptic plasticity on multiple time scales. How the dynamics of these processes interact with anti-Hebbian plasticity to shape synaptic inputs and provide a cancellation mechanism remains unclear. In the present study, we investigated the influence of parallel fiber feedback onto pyramidal neurons of the electrosensory lateral line lobe (ELL) in weakly electric fish under open loop conditions. We mimicked naturalistic parallel fiber inputs in an ELL brain slice by implementing an experimentally based model of this synaptic pathway using dynamic clamp. We showed that as parallel fiber activity increases, the effective input to ELL pyramidal neurons changes from net excitation to net inhibition, resulting in a non-monotonic firing response. Using a model neuron, we found that this robust non-monotonic response is due to a shift from balanced excitation and inhibition at low parallel fiber input rates, to dominant inhibition at high input rates. We then showed that this non-monotonic response provides a simple basis for negative image generation. Through changes in the mean activation rate of parallel fibers, the feedback can switch roles between enhancement and suppression of sensory inputs in a manner that is directly determined by the slope of the non-monotonic response curve.

Key words: disynaptic inhibition, dynamic clamp, ELL, negative image, non-monotonic response, short-term synaptic plasticity, weakly electric fish.

Introduction

Active sensing results in sensory inputs that are directly due to the sensing process (Cullen, 2004, Nelson and MacIver, 2006). Effective sensory processing requires that these self-generated (and thus redundant) inputs, also referred to as 'reafference', must be cancelled out to allow the detection of novel external inputs. In many cases, this cancellation mechanism is mediated through parallel fiber feedback from cerebellar-like brain nuclei (Bodznick et al., 1999; Bell, 2001; Cullen, 2004). This feedback provides a 'negative image' of the reafference inputs to neurons, which can then respond selectively to novel stimuli. The generation of these negative images is necessarily plastic, so that sensory systems can adapt the cancellation mechanisms to varying conditions.

Reafferent input cancellation and negative image generation have been well documented in the electrosensory system of weakly electric fish. These fish sense their environments by monitoring modulations in a self-generated electric field (Moller, 1995). The hindbrain electrosensory lateral line lobe (ELL) is the first processing stage of the electrosensory pathway. Cancellation of predictable electrosensory signals occurs, at least in part, at the level of the ELL (Bell, 2001). In mormyriform fish that produce a pulse-type electric discharge, an efference copy of the pulse is subtracted from ELL neuron responses (Bell, 2001; Bell et al., 1997; Roberts, 2000). In *Apteronotus leptorhynchus*, a gymnotiform fish that produces a high-frequency, quasi-sinusoidal electric discharge (wave-type), no efference copy of the electric discharge is available to the ELL (Bell, 2001). Instead, negative image generation in these wave-type fish relies on proprioceptive inputs and the spatiotemporal aspects of the electrosensory reafference (Bastian, 1995).

Pyramidal neurons in the ELL of gymnotiform wave-type fish receive inputs from electrosensory afferents, as well as two sources of feedback, the so-called direct and indirect feedback pathways (Berman and Maler, 1999). The indirect feedback pathway (Fig. 1) arising from cerebellar (EGp) granule cells *via* parallel fibers (Sas and Maler, 1983; Sas and Maler, 1987) mediates negative image formation (Bastian, 1995; Bell, 2001). A recent study has elegantly shown that a subset of ELL pyramidal neurons (deep pyramidal neurons, DP; Fig. 1) reliably transmits electrosensory inputs to EGp (Bastian et al., 2004). Together with proprioceptive inputs, these electrosensory inputs

to EGp control parallel fiber activity (Bastian, 1995). A distinct subset of ELL pyramidal neurons (superficial pyramidal neurons, P; Fig. 1) is the target of the parallel fiber feedback and is the primary source of electrosensory information to higher brain nuclei (Bastian et al., 2004).

Parallel fiber inputs exhibit various forms of long-term and short-term plasticity (Bastian, 1998; Lewis and Maler, 2002; Lewis and Maler, 2004). Electrical stimulation of these inputs (*in vivo* and *in vitro*) yield predominantly excitatory responses in ELL pyramidal neurons, with disynaptic inhibition providing gain control (Bastian, 1998; Berman and Maler, 1999; Lewis and Maler, 2002). Yet, models involving negative image formation rely on changes in independent inhibitory inputs (e.g. Bastian et al., 2004). While this provides a simple mechanism for negative image generation, direct inhibition is not present in parallel fiber feedback.

In the present study, we implement an experimentally based model of parallel fiber synaptic input (Lewis and Maler, 2002; Lewis and Maler, 2004) using dynamic clamp (Prinz et al., 2004), and describe its influence on ELL pyramidal neuron firing. Through a combination of experiments and modeling, we show that these synaptic inputs change from balanced excitation–inhibition to net inhibition as parallel fiber input rate increases, resulting in a non-monotonic firing response. We then show that this non-monotonic response forms a simple basis for the control and generation of a negative image of feedback inputs.

Materials and methods

In general, it is not feasible to systematically control populations of dynamic synaptic inputs. Therefore, to assess their impact on post-synaptic neuron firing we used a hybrid experimental–modeling approach in a brain slice preparation, similar in nature to previous studies (e.g. Sharp et al., 1993; Sorensen et al., 2004; Prinz et al., 2004). This so-called 'dynamic clamp' allows the delivery of an intracellular current stimulus that mimics any voltage-dependent or synaptic conductance, given that it can be described by a computer model. The important feature of this approach is that the current stimulus is modified in real-time depending on the membrane potential of the recorded neuron. Here, we extend this approach to mimic the synaptic current arising from a large population of independently firing, and plastic, parallel fiber inputs in a primary electrosensory nucleus (Fig. 1); a detailed description is provided below.

Modeling parallel fiber synaptic dynamics

FDI model

In a set of previous studies, post-synaptic potentials (PSPs) were elicited in ELL pyramidal neurons by electrical stimulation of parallel fibers (Lewis and Maler, 2002; Lewis and Maler, 2004). The PSP amplitudes (*PSP*) were described using a standard formalism (Dayan and Abbott, 2001) by the product of three simple processes (Eqn 1): facilitation (*F*), depression (*D*) and disynaptic inhibition (*DI*) – note that we use *DI* here [rather than 'I' as in Lewis and Maler (Lewis and Maler, 2002)] to avoid confusion with terminology used later (i.e. injected and synaptic currents, I_{drive} and I_{syn}).

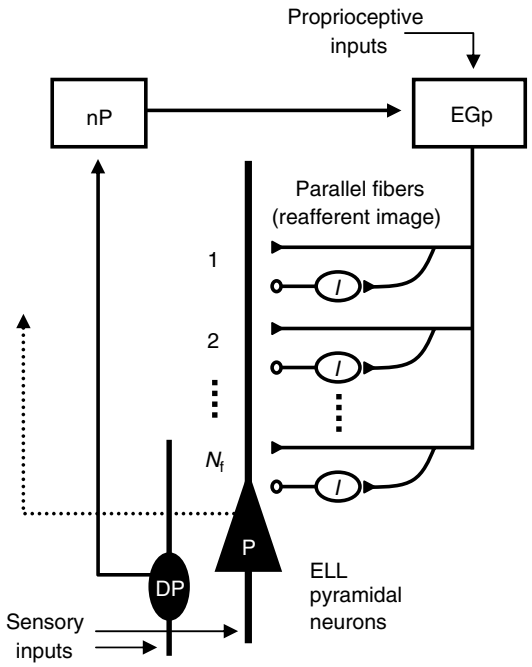

Fig. 1. The early electrosensory pathways. The schematic diagram of the ELL sub-network shows two types of principle neurons, deep (DP) and superficial (P) pyramidal neurons, as well as the primary feedback nuclei, nucleus praeminentialis (nP) and eminentia granularis posterior (EGp). The nP and EGp give rise to the direct feedback pathway (not shown) and the indirect feedback pathway (*via* parallel fibers), respectively. Feedforward input to these nuclei arises primarily from DP neurons; EGp also receives input from other sensory modalities, such as proprioception. The indirect feedback is indicated by a population of parallel fiber synaptic inputs (numbered 1 to N_f) to the P neuron, and combines direct excitation (solid triangles) with disynaptic inhibition *via* interneurons *I* (denoted by open circles). Sensory input is faithfully transmitted to parallel fibers *via* DP neurons and nP. The dynamics of the parallel fiber synapses then determine the sign of the reafferent image onto P neurons (see Results).

$$PSP_j = F_j D_j DI_j ,$$

$$\frac{dF_j(t)}{dt} = \frac{F_0 - F_j(t)}{\tau_F} \text{ and } F_j(t^*) \rightarrow F_j(t^*_-) + \Delta_F$$

$$\text{and } F_j(t^*) \rightarrow 0 \text{ if } F_j(t^*) > 0 ,$$

$$\frac{dD_j(t)}{dt} = \frac{1 - D_j(t)}{\tau_D} \text{ and } D_j(t^*) \rightarrow D_j(t^*_-) - F_j(t^*_-)D_j(t^*_-) ,$$

$$\frac{dDI_j(t)}{dt} = \frac{1 - DI_j(t)}{\tau_I} \text{ and } DI_j(t^*) \rightarrow \Delta_{FD} DI_j(t^*_-) ;$$

$$\Delta_{FD} = \frac{a\exp[-bF_j(t^*_-)D_j(t^*_-)]}{1 + a\exp[-bF_j(t^*_-)D_j(t^*_-)]} . \quad (1)$$

In Eqn 1, t^* is the time of a stimulus (or spike) in input (parallel) fiber *j* and t^*_- is the time just before. Making the update

magnitude for *DI*, Δ_{FD}, a sigmoidal function of the product *FD* [a=e^8; b=18 (see Lewis and Maler, 2002)], implements the effect of disynaptic inhibition, such that the strength of inhibition is related to the strength of its presynaptic excitation given by *FD* through a standard sigmoidal activation curve. This original model of PSP dynamics will be referred to here as the FDI model. It is important to note that the experimental conditions for which this model was developed involved synchronous stimulation of a population of parallel fibers (a so-called 'beam'), as is typical in such studies (e.g. Dittman et al., 2000). The PSP in the post-synaptic pyramidal neuron is thus a result of many individual stochastic synapses acting in concert to produce a reliable response (though variable in amplitude due to synaptic plasticity). The model therefore neglects any variability due to the stochasticity of synaptic transmission. Another important aspect of the synaptic response is that it involves overlapping excitation and inhibition (Berman and Maler, 1998a). Therefore, the update of the inhibitory process in the FDI model occurs simultaneously with that of the facilitation and depression processes (see later for further discussion of this point). In addition, by comparing synaptic responses in conditions with and without inhibition (pharmacological block), the specific effects of inhibition were quantified and reproduced by the model. The development of this model involved the assumption that the inhibitory interneurons receive the same dynamic input as the pyramidal neurons. Future studies are required to validate this assumption, but the key issue in relation to the present study is that the model reproduces the net effect of the feedback synapses (excitation and inhibition) onto the pyramidal neurons. We refer the reader to previous publications (Lewis and Maler, 2002; Lewis and Maler, 2004) for further details involved in the FDI model development and parameter fitting under the various experimental conditions.

Modeling naturalistic parallel fiber synaptic inputs

In this study, we extend the previous FDI model, which describes the discrete synaptic response amplitudes, to a conductance-based model that can be used to model naturalistic synaptic currents. We adopt an approach commonly used to combine synaptic plasticity models with conductance-based single neuron (leaky integrate-and-fire, LIF) models (e.g. Chance et al., 1998; Dayan and Abbott, 2001):

$$\frac{dV(t)}{dt} = g_o[V_o - V(t)] + I_{syn}[V(t),t] + I_{drive}\,, \tag{2}$$

$$I_{syn}[V(t),t] = G_{exc}(t)\,[V_{exc} - V(t)] + G_{inh}(t)\,[V_{inh} - V(t)]\,, \tag{3}$$

$$\frac{dG_{exc}(t)}{dt} = -\frac{G_{exc}(t)}{\tau_{exc}}\,,$$
$$\frac{dG_{inh}(t)}{dt} = -\frac{G_{inh}(t)}{\tau_{inh}}\,. \tag{4}$$

We consider a single compartment LIF model neuron (Eqn 2), with threshold (V_{thresh}) and reset (V_{reset}) values, as well as all additional parameters, provided in Table 1. The total synaptic excitatory (G_{exc}) and inhibitory (G_{inh}) conductance (and hence total synaptic current, I_{syn}) is due to the combined effects of N_f independent excitatory inputs and N_f independent inhibitory inputs respectively (Fig. 1). The dynamics of G_{exc} and G_{inh} are described by Eqn 4, except when a presynaptic input arrives, at which time they are updated using instantaneous update rules:

Table 1. *Parameter values for conductance-based synaptic model*

LIF model neuron	Synaptic conductances	FDI model
g_o=100 μS	g_{exc}=400 μS	τ_F=79 ms
V_o=–70 mV	V_{exc}=0 mV	Δ_F=0.23
V_{thresh}=–65 mV	τ_{exc}=5 ms	F_o=[0.05, 0.2]
V_{reset}=–70 mV	g_{inh}=–80 μS	τ_D=83 ms
I_{drive}=0.35 nA	V_{inh}=–80 mV	τ_I=1 s
	τ_{inh}=10 ms	N_f=120

See text for an explanation of LIF and FDI models and parameters.

Excitatory update rule:

$$G_{exc}(t^*) \rightarrow G_{exc}(t^*_-) + \frac{g_{exc}}{N_f}\,F_j(t^*_-)D_j(t^*_-)\,; \tag{5}$$

Inhibitory update rule 1:

$$G_{inh}(t^*) \rightarrow G_{inh}(t^*_-) + \frac{g_{inh}}{N_f}\,[1 - DI_j(t^*_-)]\,; \tag{6}$$

Inhibitory update rule 2:

$$G_{inh}(t^{**}) \rightarrow G_{inh}(t^{**}_-) + \frac{g_{inh}}{N_f}\,. \tag{7}$$

Excitatory update rule

When an excitatory input j fires at a time t^*, G_{exc} is increased by a discrete amount (Eqn 5) and then decays back to zero with time constant τ_{exc} (Eqn 4). This update is performed every time any of the N_f excitatory inputs fire, using the values of F_j and D_j just before their own updates (denoted by time t^*_-). The mean rate of firing in each of the N_f excitatory inputs is denoted by r_e.

We used one of two update rules for G_{inh} to account for different stimulation conditions.

Inhibitory update rule 1

The first update rule (Eqn 6) mimics the experimental conditions of the original FDI model (i.e. overlapping excitation and inhibition due to synchronous stimulation of a parallel fiber population). This method involves simulating the *DI* process in the FDI model for each of the N_f inputs. In this case, the update of G_{inh} occurs at the same times t^* as for G_{exc} using the rule described by Eqn 6. The only time we use this method is for the data fitting described in Fig. 2.

Inhibitory update rule 2

In all other aspects of the study we use a second method of updating G_{inh} that mimics spontaneous synaptic activity and asynchronous inputs – a condition that is in general not possible to reproduce using *in vitro* slice preparations. In this case, when an inhibitory input j fires at a time t^{**} (independent of excitatory input times t^*), G_{inh} is increased by a constant amount (Eqn 7). In both conditions, following the update, G_{inh} decays back to zero with time constant τ_{inh} (Eqn 4). In the second update method

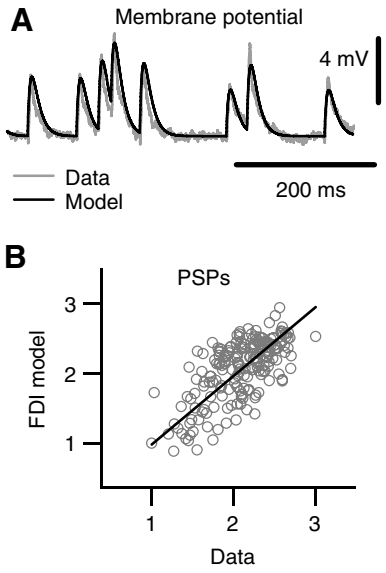

Fig. 2. Conductance-based model for the parallel fiber synapse. (A) Membrane potential trace for both model (black) and experiment (gray). (B) The predicted PSP amplitudes for the model (normalized to the first PSP in the sequence) are plotted *versus* those from an intracellular recording of an ELL pyramidal neuron using identical parallel fiber stimulation patterns (poisson-distributed inter-stimulus intervals, 16 Hz mean). Over 200 stimuli, the mean error was 17% (regression line slope=0.98, R^2=0.69). Parameter values for the model are as in Table 1, except that V_o= –77 mV.

(Eqn 7), the *DI* variable of the FDI model is not explicitly simulated. Instead, the dynamics of disynaptic inhibition are accounted for by appropriately setting the mean firing rate of each N_f inhibitory input, denoted by r_i. We take the following approach to determine r_i given a particular value of r_e.

In the context of random poisson stimulation, estimates of the mean excitatory and inhibitory conductances (G_{exc} and G_{inh}, respectively) take the form shown in Eqn 8 (Dayan and Abbott, 2001; Kuhn et al., 2004).

$$\langle G_{exc}\rangle = g_{exc}\tau_{exc}r_e\langle FD\rangle ,$$

$$\langle G_{inh}\rangle = g_{inh}\tau_{inh}r_i = g_{inh}\tau_{inh}r_e\langle 1-DI\rangle , \quad (8)$$

where $\langle x\rangle$ denotes the mean of variable x after transients have decayed (i.e. $\langle FD\rangle$ and $\langle 1-DI\rangle$ are the quantities shown in Fig. 4A as a function of r_e; for convenience, we define $\langle I_D\rangle=\langle 1-DI\rangle$ as the variable describing the strength of disynaptic inhibition). From this, we can explicitly model the rate of the inhibitory inputs (r_i) as a function of r_e ($r_i=r_e\langle I_D\rangle$). Thus, the mean rate of inhibitory input is dependent on the excitatory input (to model the disynaptic inhibition); however, all individual inputs are temporally uncorrelated (i.e. are driven by independent poisson processes). While this relationship is explicitly derived from the original experimentally based FDI model, it can also be thought of as a simple rate model of disynaptic inhibition, in which the mean rate of inhibition r_i is a sigmoidal function of the mean rate of excitation, r_e. This simplification was used to increase the efficiency of the dynamic clamp implementation in the experiments (see below). While it was not necessary for the simulation studies, for consistency the same model was used throughout with only minor (quantitative) effects on our results. That said, this formulation may not hold in different conditions involving strong coherent activity among inputs.

All parameter values are presented in Table 1; any values different from these are mentioned in the text as necessary. Simulations were performed using a semi-analytic method for the FDI variables (Lewis and Maler, 2002) and an Euler integration method for the conductance-based LIF model (time step=0.2 ms); both were implemented in Igor Pro (Wavemetrics Inc., Lake Oswego, OR, USA) and Matlab (The Mathworks Inc., Natick, MA, USA).

Condition for balanced excitation and inhibition

The condition such that excitation and inhibition exist in balance is typically determined by setting the current–balance equation (Eqn 2 and Eqn 3) to zero and assuming the membrane voltage and synaptic conductances take on their mean values, Eqn 9 (e.g. Kuhn et al., 2004):

$$0 = g_o(V_o-\langle V\rangle) + \langle G_{exc}\rangle(V_{exc}-\langle V\rangle) + \langle G_{inh}\rangle(V_{inh}-\langle V\rangle) + I_{drive} . \quad (9)$$

Substituting Eqn 8 and solving for r_i gives the condition for balanced inhibition (Eqn 10):

$$r_i = \left[\frac{g_o(V_o-\langle V\rangle)+I_{drive}}{g_{inh}\tau_{inh}(\langle V\rangle - V_{inh})}\right] + r_e\langle FD\rangle\left[\frac{g_{exc}\tau_{exc}(V_{exc}-\langle V\rangle)}{g_{inh}\tau_{inh}(\langle V\rangle - V_{inh})}\right] . \quad (10)$$

ELL slice preparation and intracellular dynamic clamp

Surgical procedures and slice preparation were performed as previously described (Berman and Maler, 1998b; Lewis and Maler, 2002). Briefly, the gymnotiform fish *Apteronotus leptorhynchus* (Eigenmann) (male or female, 10–15 cm in length) were anesthetized in oxygenated water containing 0.2% tricaine methanesulfonate (Syndel International Inc., Vancouver, BC, Canada). True-transverse 350 μm slices of the electrosensory lateral line lobe (ELL) were obtained using an OTS-5000 tissue slicer (FHC Inc., Bowdoin, ME, USA) and transferred to an interface-type slice chamber (Scientific Systems Design Inc., Mississuaga, ON, Canada). Slices were perfused (2 ml min^{-1}) with artificial cerebrospinal fluid (ACSF), bubbled at room-temperature (20–22°C) with a mixture of 95% O_2/5% CO_2, and containing (in mmol l^{-1}) 124 NaCl, 24 $NaHCO_3$, 10 D-glucose, 1.25 KH_2PO_4, 2 KCl, 2 $CaCl_2$, 2 $MgSO_4$. A recovery period of at least 1 h was allowed before recordings were made. Protocols were approved by the University of Ottawa Animal Care Committee (BL-191).

Intracellular recordings from pyramidal neurons in the centromedial segment of ELL were obtained using sharp microelectrodes (~80 MΩ) and an Axoclamp-2B amplifier (Molecular Devices, Sunnyvale, CA, USA) in discontinuous-current-clamp (DCC) mode at a 3–4 kHz switching rate. Only neurons whose spontaneous firing rate was between 0.5–6 Hz were used in this study; sometimes a small constant current (<0.5 nA) was used to maintain this spontaneous rate over the

duration of the recordings (baseline membrane potential 69±0.9 mV; input resistance 58±6 MΩ). We use the dynamic clamp approach (Sharp et al., 1993; Prinz et al., 2004) to assess the effects of model synaptic inputs on pyramidal neurons. The dynamic clamp was implemented using models constructed in Simulink and Real-Time Workshop (Matlab) and run on a DS1104 controller board (dSpace Inc., Wixom, MI, USA), as described previously (Sorensen et al., 2004). Membrane voltage was acquired and used in the real-time simulations to update intracellular current injection (determined by the sum of all excitatory and inhibitory conductances, see Eqn 3) at a rate of 5 kHz. This injected current is sometimes referred to as 'injected conductance' due to its dependence on the specified driving forces. The dynamics of the *F* and *D* processes (Eqn 1) for each of N_f independently firing poisson inputs were simulated. Similar to our previous studies, we solve for *F* and *D* using a semi-analytic method for faster computations (Lewis and Maler, 2002; Lewis and Maler, 2004). In addition, we used either the original model (full simulation of *I* dynamics) or the simplified description of inhibition ($r_i=r_e<I_D>$) described in the previous section. This simplified relationship between r_i and r_e was determined offline for a given parameter set and then implemented in the dynamic clamp using a lookup table. While not necessary to implement the dynamic clamp in real-time, because of its relative simplicity, this method allows a faster sampling and update frequency. To assess the response of a pyramidal neuron to a given input rate r_e, the dynamic clamp synapses were first activated and then 20–30 s later (allowing transients to decay), 10 s of data were acquired. The firing rate was calculated over this 10 s interval. This was repeated 3–5 times and averaged for each value of r_e for each neuron. Values of r_e were varied randomly and not all values of r_e were sampled in all neurons; for display of mean responses, data were binned in 2 Hz intervals of r_e, and presented as mean ± s.d. (standard deviation) unless otherwise indicated.

Investigating negative image generation

To investigate the functional consequences of dynamic parallel fiber inputs on ELL pyramidal neurons, we adopt an approach based on previous studies involving negative image generation during sinusoidal spatially global stimulus presentation (Bastian, 1995; Nelson and Paulin, 1995; Bastian et al., 2004). Such stimulation mimics predictable signals produced for example by an animal's own movements. We assume that such sinusoidal signals are faithfully transmitted through the different processing stages (see Fig. 1) and represented accurately in a rate modulation of parallel fiber activity (Bastian et al., 2004). Thus, in our study, negative image generation is directly related to parallel fiber dynamics (with associated disynaptic inhibition). These presynaptic effects will necessarily interact with the well-described and critically important effects of postsynaptic processes (Bastian, 1998). Our approach is open-loop, such that the effect of the feedback alone can be considered, so no time delays are involved. Under more natural (and complex) closed-loop conditions, in which primary sensory input is combined with feedback input, the feedback delay will be important, especially for higher frequency modulations.

As is the convention, we quantify neural responses to sinusoidal inputs in terms of the phase histogram (e.g. Bastian et al., 2004). In such plots, spike times are binned and counted relative to the phase of the sinusoidal input at which they occur. Phase histograms indicate the degree to which a neuron follows a sinusoidal input, and can be further quantified in terms of the 'vector strength' and 'preferred phase' (Batschelet, 1981). These quantities are determined by the magnitude and phase, respectively, of the resultant vector calculated from the vector sum of bin phases weighted by the bin height (in polar coordinates). The vector strength varies from 0 (no phase preference) to 1 (perfect phase locking), and here we consider the preferred phase to vary from –180° to +180°, where a phase of +90° corresponds to a response that is exactly 'in-phase' with the input and a phase of –90° is exactly 'anti-phase' (since the sine wave input attains a minimum at –90°). Both model simulations and experimental recordings were analyzed in the same way. Values are presented as mean ± s.d. unless otherwise indicated.

Results

Conductance-based model of parallel fiber synaptic inputs

The dynamics of synaptic responses are typically modeled using a combination of facilitation-like processes (that increase response amplitude) and depression-like processes (that decrease response amplitude) – the so-called *FD* formalism (Dayan and Abbott, 2001). These models describe synaptic dynamics in terms of a sequence of response amplitudes. Such an approach has been previously used to describe the parallel fiber synapses onto ELL pyramidal neurons under a variety of conditions (Lewis and Maler, 2002; Lewis and Maler, 2004). Briefly, the direct excitatory input from parallel fibers onto pyramidal neurons is modeled by the product of a facilitation term (*F*) and a depression term (*D*). The disynaptic inhibition *via* interneurons is modeled by a depression-like term (*DI*) that depends on the product *FD* (see Eqn 1). While this model is sufficient for describing the sequences of PSP amplitudes evoked by synchronous stimulation of a population of parallel fibers in slice experiments, a modified approach is required to evaluate the effects of plasticity on the 'synaptic currents' produced by a population of asynchronously firing parallel fiber inputs. To this end, we extended the previous FDI model to a conductance-based description (Eqn 2–8).

Because the previous FDI model already captures the variation in PSP amplitudes, the associated parameters were fixed to their original experimentally determined values (Eqn 1, Table 1) (Lewis and Maler, 2002; Lewis and Maler, 2004); these parameter values are considered the best fit parameters over several different experiments (N=7–12, depending on the stimulation protocol) using both extracellular field potential and intracellular recordings. It is straightforward to fit the new synaptic model to the data from intracellular recordings (N=3; R^2>0.69) with reasonable choices for the new parameters associated with an LIF model neuron (Eqn 2–7). Fig. 2 shows a comparison of the conductance-based parallel fiber synapse model to intracellular recordings obtained from a pyramidal neuron in an ELL brain slice. For a sequence of 200 parallel fiber stimuli delivered at random intervals (16 Hz mean rate), the model provides a good estimate of the intracellular PSP amplitudes (R^2=0.69; Fig. 2B). The LIF parameters used in this example were adopted for all of the neuron model simulations described below (unless otherwise noted); see Table 1. It is

important to note that this choice of parameter values does not influence the results of our study, as will become apparent for the model-data comparison in following sections.

Parallel fiber synaptic inputs produce a non-monotonic response in pyramidal neurons

We now investigate the effects of naturalistic synaptic inputs from a population of parallel fibers on ELL pyramidal neuron firing rate. In general it is not possible to mimic such synaptic input in brain slice preparations with electrical stimulation, so we experimentally implement the parallel fiber synapse model using dynamic clamp. In the previous section, all inputs were considered to fire synchronously (as is the case with direct electrical stimulation of parallel fibers in the experiments). We now assume that each of the 120 excitatory inputs fires independently at a mean poisson rate, r_e. Another 120 inhibitory inputs fire at a rate $r_i=r_e\langle I_D\rangle$ (see Materials and methods). Fig. 3 shows the effects of increasing r_e on the normalized firing rate of pyramidal neurons. Fig. 3A,B illustrates a clear decrease in firing rate in one neuron as r_e increases from 5 Hz to 20 Hz. This general effect was seen in all neurons. From the mean response function (Fig. 3C; mean ± s.d.; N=16), it is clear that pyramidal neuron firing rate first increases to a maximum, and then decreases with further increases in r_e. This non-monotonic response was also observed for other parameter sets, as well as in a series of experiments where the full FDI model was simulated (i.e. explicit simulation of the *DI* process; data not shown). In the following, using simulations, we investigate the mechanisms underlying this non-monotonic response in more detail.

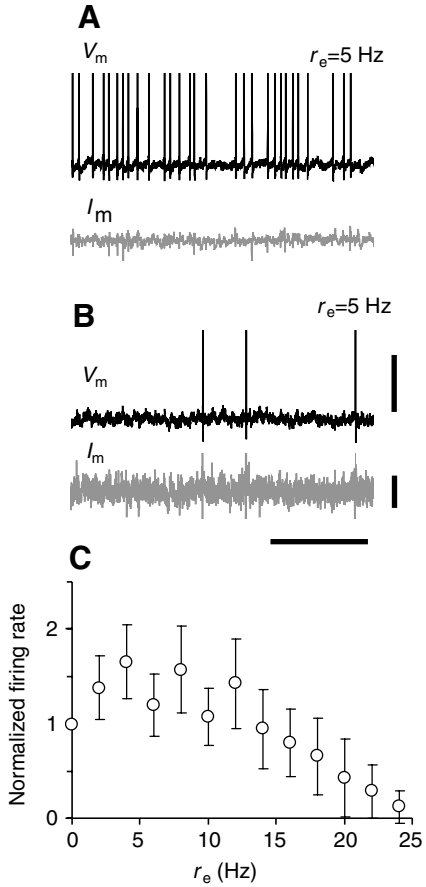

Fig. 3. Dynamic clamp studies showing non-monotonic firing response. (A,B) Example traces from one ELL pyramidal neuron showing membrane potential (black, V_m) and injected current (gray, I_m) for two different values of r_e (5 Hz and 20 Hz). Scale bars are the same for both A and B (40 mV, 0.4 nA, 1 s). (C) Non-monotonic firing response of ELL pyramidal neurons; normalized mean firing rate (mean ± s.d.; 16 neurons) is shown as a function of mean excitation rate, r_e (binned in 2 Hz increments).

Parallel fiber synaptic dynamics: FDI model

We now consider the effects of asynchronous inputs from a population of parallel fibers on the steady-state behavior of the parallel fiber synaptic model. Fig. 4 shows how the three variables of the FDI model change as a function of the mean poisson rate of 120 independent inputs, r_e. In these simulations, the inhibitory process was simulated explicitly (I_D=1–*DI*); see Materials and methods (Lewis and Maler, 2002). The product *FD* increases with r_e to a slight maximum and then decreases as depression becomes dominant. Although the inhibitory term I_D is related to the product *FD*, it increases monotonically over this range of r_e. This description provides the basis for the simplification used in the conductance-based model. As described in the Materials and methods, the FDI model was developed for synchronous inputs that produce overlapping EPSPs and IPSPs, and does not explicitly involve independent disynaptic inhibitory inputs. Rather, the influence of inhibition is related to the level of excitation (given by the product *FD*). Assuming a steady-state value of inhibition (I_D) as a function of r_e (Fig. 4A), we can relate r_i to r_e ($r_i=r_e\langle I_D\rangle$; see Materials and methods for details). In all further analyses, we adopt this relationship to describe disynaptic inhibition, as it allows us to study the effects of asynchronous randomly firing inputs.

Synaptic dynamics, balanced inhibition, and a non-monotonic firing response

Many studies have considered background synaptic activity arising from balanced excitation and inhibition (e.g. Chance et al., 2002; Kuhn et al., 2004). In such scenarios, the parameters determining the net excitatory and inhibitory conductances are chosen so that there is no change in mean membrane potential. The 'balanced' condition dictates a rate of inhibition, given a particular rate of excitation (Eqn 10). Fig. 4B compares the level of inhibition determined by the parallel fiber synapse model with that determined by the balanced condition. The inhibitory rate for the balanced condition was determined from Eqn 10 using the value of $\langle FD\rangle$ for a given value of r_e (Fig. 4A); all other parameters were identical in the two cases. Thus, the level of excitation is identical in the two different cases so a direct comparison of inhibition levels can be made. For low values of r_e, the FDI conductance-based model and the balanced condition result in similar levels of inhibitory input rates (Fig. 4B). For high r_e, the inhibitory rates in the two cases diverge, with the FDI model producing relatively higher values of inhibition.

Importantly, the excitation–inhibition balance in the parallel fiber synapse model is also reflected in the average membrane potential of a model LIF neuron, over a similar range of r_e (Fig. 4C, compare solid and dotted lines). There is a relatively

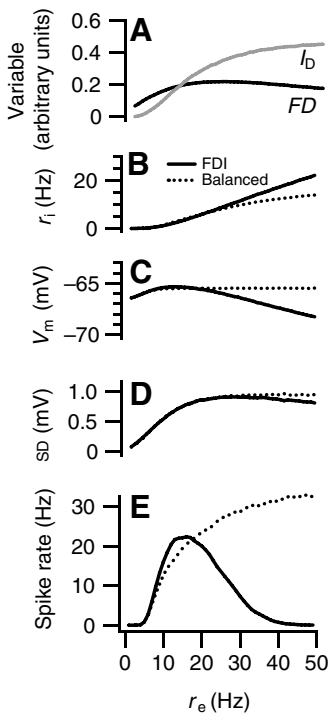

Fig. 4. Basis of non-monotonic firing in an LIF model neuron. (A) Changes in FDI model variables with excitation rate, r_e. *FD* (black) denotes the product of the facilitation and depression variables and I_D (gray) denotes the inhibition variable (see Materials and methods for details). Values plotted are means for 120 independent inputs over 30 s of simulation time. (B) The effective rate of inhibition, r_i, as a function of excitation rate, r_e, for the FDI conductance-based model (solid line); for comparison, the inhibition rate at which excitation and inhibition is balanced is also indicated (dotted line). (C) Mean and (D) standard deviation of the membrane potential in the LIF neuron as a function of excitation rate, r_e. Also shown are the values resulting from the balanced condition (dotted lines, as in B). (E) Spike rate of the LIF neuron as a function of excitation rate, r_e, showing non-monotonic response profile; spike rate resulting from the balanced condition is also shown (dotted line, as in B; see Materials and methods for details). Values plotted in C–E are means over 20 simulated trials of 20 s of simulation time for 120 excitatory and 120 inhibitory inputs (standard errors are less than the line width). For all panels, F_o=0.05, with other parameter values provided in Table 1.

large decrease in membrane potential for higher r_e. There is also a decrease in the absolute level of fluctuations in membrane potential compared to the balanced condition (Fig. 4D). Membrane fluctuations can greatly influence the firing response of a neuron (Longtin et al., 2002; Kuhn et al., 2004), so these effects will contribute to differences in the firing rate of neurons receiving balanced *versus* unbalanced inhibition.

Overall, the variations in membrane potential shown in Fig. 4C,D lead to a non-monotonic response in the firing rate of the LIF model as well (Fig. 4E). Over the range of r_e considered here, a similar response is not evident for the balanced condition. For much higher input rates, however, the effects of inhibitory shunting can dominate, resulting in a non-monotonic response for the balanced condition as well (Kuhn et al., 2004).

The nature of the non-monotonic response observed in the parallel fiber synapse model can vary with changes in model parameters. Of particular interest is the parameter F_o, which describes the initial release probability of a synapse (Abbott and Regehr, 2004). We have previously shown that changes in F_o alone were sufficient to explain a long-term synaptic enhancement (LTE) exhibited by parallel fiber inputs onto ELL pyramidal neurons (Lewis and Maler, 2004). Thus by varying F_o over the range found experimentally (F_o=0.05–0.2), we can assess how LTE influences the effects of parallel fiber synaptic inputs. For F_o=0.2, the firing rate response remains non-monotonic (see Fig. 6C, gray curve), but the peak firing rate occurs at a lower value of r_e than in Fig. 4E (F_o=0.05). This is because inhibition becomes dominant and thus diverges from the balanced condition at lower values of r_e (data not shown). Therefore, LTE provides a mechanism for modulating quantitatively the non-monotonic firing response.

We also observed non-monotonic responses for other parameters in the LIF neuron model. Increases in I_{drive} cause the neuron to fire at finite rates for minimal or absent parallel fiber input. This results in response curves that are shifted upwards for low values of r_e, but the non-monotonic behavior remains. Similarly, decreases in I_{drive} result in a downward shift in the response curves. Indeed, much of the variability in the responses of ELL pyramidal neurons (cf. error bars in Fig. 3C) can be attributed to differences in threshold and spontaneous firing rate. The non-monotonic response is robust, however, because it is due to a systematic shift from excitation to inhibition, rather than requiring a delicate balance between them.

A non-monotonic firing response provides a framework for negative image generation

In this section, we consider the implications of a non-monotonic firing response in the context of reafference input cancellation by parallel fiber inputs. We followed the approach of several previous studies by modeling the reafference signal as a low-frequency global amplitude modulation, produced for instance by tail-bending or breathing movements (e.g. Bastian, 1995; Nelson and Paulin, 1995; Bastian et al., 2004). In particular, we chose a 1 Hz sinusoidal modulation, and assume that this reafference signal is transmitted reliably by DP neurons in the ELL, through nP and EGp, resulting in a sinusoidal rate-modulation of parallel fiber activity (see Fig. 1) (Bastian et al., 2004). In this scenario, we consider only the effect of parallel fiber inputs (i.e. the feedback image) and not the combination of this image with the primary sensory inputs. In other words, we are concerned only with image generation by parallel fiber feedback.

The non-monotonic firing responses (Figs 3 and 4) show that depending on the baseline rate (r_e) of parallel fiber inputs, the net effect of small increases in rate can effectively be either excitatory (increase pyramidal neuron firing rate) or inhibitory (decrease pyramidal neuron firing rate). In other words, either a positive or a negative image can be transmitted by parallel fibers, depending on their state (i.e. baseline firing rate r_e). Fig. 5 illustrates this simple idea in both LIF neurons (model) and ELL pyramidal neurons (data). The sinusoidal input signal is a rate modulation (r_e±5 Hz) and is illustrated in Fig. 5D. The phase histograms (of spiking) for different baseline rates r_e are shown in Fig. 5A–C. For r_e=10 Hz, it is clear that most spikes occur 'in phase' with the input (positive image), while for r_e=25 Hz, most spikes occur

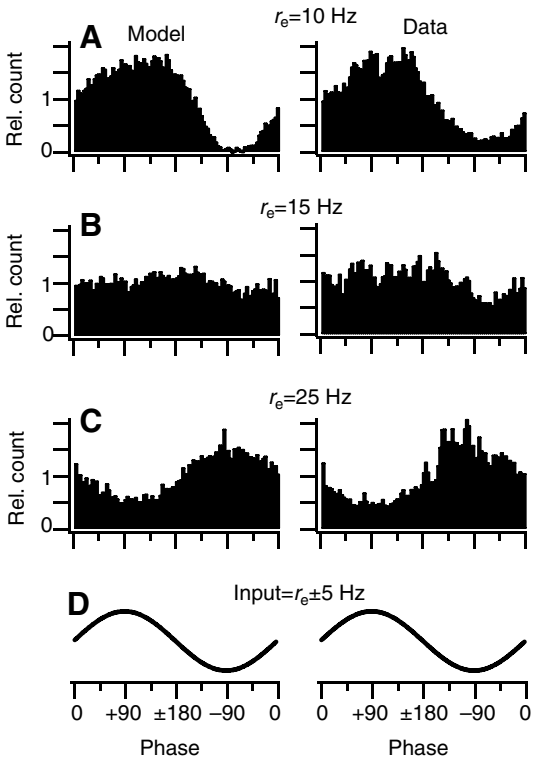

Fig. 5. Negative image generation in ELL pyramidal neurons (right panels) and LIF model neurons (left panels). Spiking response to 1 Hz sinusoidal modulation of parallel fiber rate, r_e±5 Hz; denoted schematically in (D). (A–C) Phase histograms as the baseline input rate of the modulation r_e increases from 10 Hz to 25 Hz. Over this range, the phase histograms in both model and experiment indicate a change from in-phase responses to out-of-phase responses. Histograms were computed for 10 000 spikes in the model, and the combined responses of five pyramidal neurons (individual neuron responses are quantified in Fig. 6). Parameter values are as in Fig. 4.

'out of phase' with the input (negative image). At an intermediate baseline rate r_e=15 Hz, very little phase locking is observed. Similar results are observed in both model and experiments (Fig. 5, compare left and right panels).

We have quantified these responses in the conventional manner by calculating the vector strength of the spiking response to the sinusoidal input (see Materials and methods); a vector strength of 1 indicates perfect phase locking, while a value of zero indicates no phase locking. In addition, we compute the preferred phase, relative to the input signal; a negative phase denotes out-of-phase spiking. The data (open symbols, mean ± s.d., N=5 neurons) and model (solid black line) show a very close correspondence (Fig. 6A,B; F_o=0.05), and clearly indicate the switch from positive image to negative image around r_e=15 Hz. At this transition point, the phase values for the data were highly variable and the vector strength relatively low. Also shown (Fig. 6A,B; gray lines) are model calculations for a different value of the parameter F_o=0.2 (recall that this is associated with a long-term synaptic plasticity). Changing F_o shifts the transition point for negative image generation to lower values of parallel fiber baseline rate.

These results can be qualitatively summarized in terms of the non-monotonic response curves (Fig. 6C). The slope of these curves determines the sign of the feedback image: positive images are generated for low values of r_e that correspond to a positive slope, and negative images are generated for high values of r_e that correspond to a negative slope. In an intermediate range, either sign can result or the input can be filtered out from the feedback entirely, depending on the r_e and parameters such as F_o. Overall, this provides a simple explanation, using a bottom-up approach, of how parallel fiber activity can generate a negative image of a reafference signal.

Discussion

Reafference suppression and negative image generation are important aspects of electrosensory system function (Bell, 2001; Bodznick et al., 1999; Bastian and Zakon, 2005) and the underlying post-synaptic mechanisms are well-known (Bell, 2001; Bastian, 1999). In our study, we show how presynaptic mechanisms, determined by short-term plasticity and disynaptic inhibition, can also provide an important contribution to negative image generation.

In previous studies (Lewis and Maler, 2002; Lewis and Maler, 2004), we developed a model of the synaptic dynamics resulting from stimulation of the parallel fiber feedback pathway in the electrosensory lateral line lobe (ELL). The model, which described the dynamics in terms of post-synaptic response amplitudes, was based on the short-term plasticity (facilitation and depression) and disynaptic inhibition involved in the parallel fiber feedback. In the present paper, we extend this model to a conductance-based description. In doing so, we were able to investigate the effects of more naturalistic input from this feedback pathway on ELL pyramidal neurons using dynamic clamp.

Dynamic clamp, synaptic plasticity and naturalistic inputs

Typically, synaptic dynamics are characterized using *in vitro* preparations, in which greater experimental control is feasible. But in the context of naturalistic feedback, such studies are limited because either (1) synaptic inputs are activated through the synchronous electrical stimulation of large populations of synapses, or (2) minimal stimulation is used, such that only individual synapses are activated. *In vivo* synaptic activity is often generated by populations of asynchronously firing synaptic inputs that are more difficult to study experimentally, and have so far been primarily addressed using synaptic inputs simulated with the dynamic clamp technique (e.g. Chance et al., 2002; Prinz et al., 2004; Wolfart et al., 2005).

The dynamic clamp technique has proved to be a powerful tool for the investigation of both single neuron dynamics as well as simple networks (Prinz et al., 2004). Many previous studies have used dynamic clamp to simulate synaptic activity (e.g. Chance et al., 2002; Desai and Walcott, 2006; Fellous et al., 2003; Wolfart et al., 2005), and some others have simulated different forms of synaptic plasticity (Rabbah and Nadim, 2005; Nowotny et al., 2006; Mittmann and Hausser, 2007). However, to our knowledge, no other study has considered the contributions of synaptic plasticity to the effects of large populations of independent synaptic inputs with independent dynamics. Our ability to achieve this

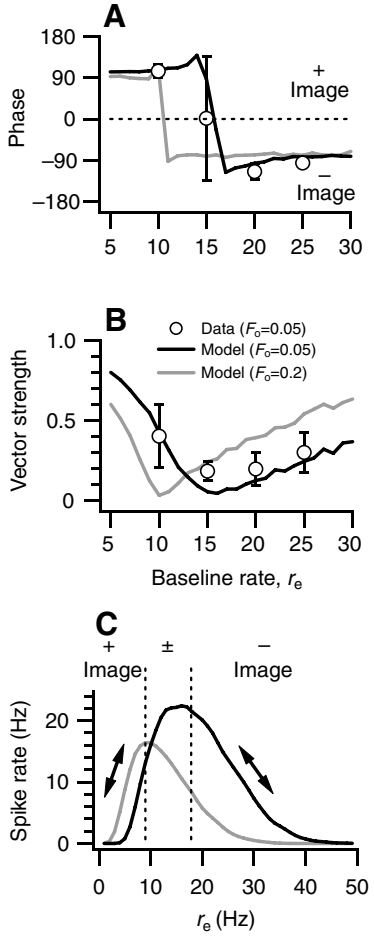

Fig. 6. Quantification of the negative image response as a function of baseline input rate r_e. (A,B) Phase histograms were quantified in terms of the preferred phase (A) and the vector strength (B). Each panel shows the results for both model (F_o=0.05 in black, F_o=0.2 in gray) and experiment (F_o=0.05, open symbols; mean ± s.d., N=5 neurons). As indicated, a positive preferred phase represents an in-phase response and a negative preferred phase represents an out-of-phase response (i.e. negative image). (C) Similar to Fig. 4E, the firing rate response of the LIF model is shown for F_o=0.05 (black) and F_o=0.2 (gray). Also indicated are the regions of r_e in which the preferred phases are positive and negative (plus-image and minus-image respectively). Note that this corresponds to the sign of the slope of the non-monotonic response curve. Also note that for intermediate values of r_e the responses depend on F_o and are characterized by preferred phases of either sign and relatively low vector strength.

computationally demanding task was a result of the particular method of implementing dynamic clamp, in addition to our semi-analytic description of synaptic dynamics (see Materials and methods). Of course, some caution must be taken when interpreting the results of any dynamic clamp study, because recording and current injection are made at a single location in a neuron (usually the soma). The potential effects of the spatial distribution of the synapses are ignored, though the extent to which this is a problem will be neuron-dependent. Recent studies have suggested that neurons may be electrically more compact than previously thought, so even distant dendritic events can influence somatic activity (Marder, 2006).

Non-monotonic firing responses

We found, in our studies, that due to the dynamics of facilitation, depression and disynaptic inhibition, the effect of parallel fiber input on ELL pyramidal neuron firing changes from net excitation to net inhibition as input rates increase. The resulting non-monotonic response in pyramidal neuron firing is similar to that described in other studies, involving both experimental and modeling contexts (e.g. Wu et al., 2006; Tan et al., 2007; Mikula and Niebur, 2003; Kuhn et al., 2004; de la Rocha and Parga, 2005). However, the underlying mechanisms vary. In cases where correlations are present in the input, synaptic depression effectively decorrelates the high frequency inputs resulting in a decreased output rate (and a non-monotonic response) as input frequency rises (Mikula and Niebur, 2003; de la Rocha and Parga, 2005). Kuhn et al. (Kuhn et al., 2004) described a non-monotonic response function that results from a different mechanism. Using a conductance-based LIF neuron model with balanced excitation–inhibition, they showed that the increased total conductance resulting from increased input rate produces competing effects: a decreased membrane time constant leads to an increase in output firing rate through increased membrane transients, while an increased shunting effect tends to decrease output firing rate through decreased membrane fluctuations. The mechanisms outlined could also play a role in our parallel fiber synapse model, depending on the conditions. However, the primary mechanism underlying the non-monotonic response described here is the change in the balance of excitation–inhibition resulting from increased disynaptic inhibition at higher input rates.

Several computational advantages of non-monotonic neuronal response functions have been reviewed recently (Kuhn et al., 2004; de la Rocha and Parga, 2005). For example, it allows neurons to be in a firing state far from saturation, such that changes in input rates can be encoded over a wide range of average rates. A non-monotonic response function can also provide specific input tuning, such that a neuron will have a preferred range of input rates, or frequency selectivity. If different neurons exhibit differently shaped response functions, they can form the basis for a population code (Sanger, 2003). Tan et al. (Tan et al., 2007) have recently shown that non-monotonic responses resulting from changes in excitatory–inhibitory balance can form an auditory population code for sound intensity. A similar diversity of response curves in ELL could result from a diversity of baseline firing rates among parallel fibers.

Implications of non-monotonic response in ELL: negative image generation

In gymnotiform fish, pyramidal neurons of the electrosensory lateral line lobe provide the primary source of electrosensory information to all other brain regions. Pyramidal neuron dynamics and encoding have been extensively studied in recent years (Oswald et al., 2004; Doiron et al., 2001; Chacron et al., 2003). In addition, the functional roles of feedback have also been recently studied in different contexts (Doiron et al., 2003; Bastian et al., 2004). In particular, the parallel fiber feedback pathway to ELL is responsible for cancelling out reafferent or redundant sensory inputs (Bell, 2001; Bastian, 1995). When spatially local and spatially global sinusoidal stimuli are paired,

some pyramidal neurons gradually adapt their firing so that afterwards, the global stimulus alone produces a response that is 180° out of phase compared to before pairing, a so-called 'negative image' of the stimulus (Bastian, 1998). The model mechanism proposed in Bastian et al. (Bastian et al., 2004) involved anti-Hebbian plasticity and activation of feedback excitation and inhibition that were independent (for simplicity). In addition, the model predicted that a parallel but non-plastic feedback pathway should act as a 'teacher' to guide the adaptive plasticity – remarkably this was confirmed in the anatomy. Our studies provide an extension to this model while maintaining more realistic circuitry (i.e. disynaptic inhibition rather than independent inhibition). Previous work has shown that a presynaptic potentiation occurs during the pairing-protocol (Bastian, 1998). This is similar to the LTE we discuss here, which results in a shift of the pyramidal neuron response function, as in Fig. 6C. This in turn would lead to inhibition being dominant at lower rates and enhancing the effect of the negative image. In addition, a pairing-specific shift in inhibitory gain (due to postsynaptic mechanisms) would be involved so that the requirement for independent excitation and inhibition is not necessary. Presynaptic potentiation has also been observed in the parallel fiber feedback pathway in pulse-type fish (e.g. Bell et al., 1997) and thus could play a similar role in shaping negative image formation.

The parallel fiber feedback to ELL has also been shown to be involved in gain control (Bastian, 1986). A recent study has suggested a mechanism for this gain control that involves the activation of inhibition in combination with an excitatory mechanism resulting from the intrinsic neural dynamics (Mehaffey et al., 2005). Though the effect of excitatory synapses was not considered, the inhibition was assumed to arise through the disynaptic inhibition in the parallel fiber feedback pathway. Our results suggest that this mechanism would be operating for high enough rates of activity in parallel fiber inputs, when inhibition is dominant.

Balancing synaptic inputs with disynaptic inhibition

Most studies involving so-called balanced excitation and inhibition have been performed *ad hoc*. How such balancing is achieved in general by networks is not clear. The relationship typically used to determine the balanced condition (Eqn 10) specifies the level of inhibition required to balance excitation at a particular (mean) membrane potential. Recent *in vivo* studies have shown that balanced input can result in part from disynaptic feedforward inhibition during active sensory processing (Higley and Contreras, 2006). Our results also show that disynaptic inhibition can play a role in balancing synaptic activity. Our parallel fiber model produces balanced synaptic activity for low input rates (Fig. 4). At higher rates, inhibition becomes dominant and the synaptic input is no longer balanced. In a different parameter regime, a similar synaptic pathway consisting of excitation and disynaptic inhibition could implement the balanced condition over a larger range of input rates. The requirement for balanced inhibition is that the input–output relationship at the inhibitory interneuron is similar to Eqn 10. Thus, for robust balancing to occur (i.e. over a large range of membrane potentials), voltage-dependent post-synaptic mechanisms would also be required, otherwise even small changes in average membrane potential will result in a net synaptic input that is unbalanced. Possible mechanisms could involve nonlinear amplification of PSPs by persistent Na^+ currents (Fortune and Rose, 2003) or voltage-dependent synaptic inhibition, both of which have been observed in parallel fiber feedback to ELL pyramidal neurons (Berman and Maler, 1998a; Berman et al., 2001).

Future directions

Our studies of the parallel fiber feedback pathway in the electrosensory system suggest a presynaptic contribution to the generation of the negative image that is so important for cancelling redundant sensory inputs. The synaptic activity resulting from an interaction between short-term plasticity and the relative levels of excitation and inhibition provides a simple framework for the generation and the control of the negative image. Because of the generality and ubiquity of the features underlying this framework, it is very possible that similar mechanisms for sensory filtering and cancellation are at work in other sensory systems.

However, many questions remain regarding the functional role of parallel fiber feedback to ELL. For one, it is clear that the baseline firing rate of the parallel fibers can be very important, allowing them to toggle between excitatory to inhibitory. While we have discussed their role in negative image generation, it is also possible that they provide positive feedback. At this time, it is not clear what role this type of feedback could play. Indeed, it is also not clear how parallel fiber firing patterns *in vivo* vary under natural conditions, but the framework outlined here should guide these future experiments. On another note, the synaptic dynamics in this study are modeled in a phenomenological context. Further experiments are also required to determine the exact mechanisms of facilitation, depression and, perhaps most importantly, the role of the inhibitory interneurons in shaping the synaptic dynamics. This knowledge will allow the targeted manipulations required during *in vivo* experiments to fully understand the role of dynamic feedback in closed-loop sensory processing.

List of abbreviations

ACSF	artificial cerebrospinal fluid
D	depression
DCC	discontinuous-current-clamp
DI	disynaptic inhibition
DP	deep pyramidal neuron
EGp	eminentia granularis posterior
ELL	electrosensory lateral line lobe
EPSP	excitatory synaptic potential
F	facilitation
G_{exc}, G_{inh}	excitatory, inhibitory synaptic conductance
I_{drive}	constant injected current
IPSP	inhibitory synaptic potential
I_{syn}	synaptic current
LIF	leaky integrate-and-fire
LTE	long-term synaptic enhancement
P	superficial pyramidal neuron
PSP	post-synaptic potential
PSP	PSP amplitude

V_{reset}	reset voltage
V_{thresh}	threshold voltage
nP	nucleus praeminentialis

Thanks to Michael Sorenson and Ron Calabrese for introducing us to the dSpace Inc. system for implementing the dynamic clamp. This research was supported by grants to J.E.L. from the Canadian Institutes of Health Research (Senior Research Fellowship), Canadian Foundation for Innovation (New Opportunities Fund), Ontario Innovation Trust, as well as start-up funds from the University of Ottawa.

References

Abbott, L. F. and Regehr, W. G. (2004). Synaptic computation. *Nature* **431**, 796-803.

Bastian, J. (1986). Gain control in the electrosensory system: a role for the descending projections to the electrosensory lateral line lobe. *J. Comp. Physiol. A* **158**, 505-515.

Bastian, J. (1995). Pyramidal-cell plasticity in weakly electric fish: a mechanism for attenuating responses to reafferent electrosensory inputs. *J. Comp. Physiol. A* **176**, 63-78.

Bastian, J. (1998). Plasticity in an electrosensory system. III. Contrasting properties of spatially segregated dendritic inputs. *J. Neurophysiol.* **79**, 1839-1857.

Bastian, J. (1999). Plasticity of feedback inputs in the apteronotid electrosensory system. *J. Exp. Biol.* **202**, 1327-1337.

Bastian, J. and Zakon, H. H. (2005). Plasticity of sense organs and brain. In *Electroreception* (*Springer Handbook of Auditory Research, Vol. 21*) (ed. T. H. Bullock, C. D. Hopkins, A. N. Popper and R. R. Fay), pp. 195-228. New York: Springer.

Bastian, J., Chacron, M. J. and Maler, L. (2004). Plastic and nonplastic pyramidal cells perform unique roles in a network capable of adaptive redundancy reduction. *Neuron* **41**, 767-779.

Batschelet, E. (1981). *Circular Statistics in Biology*. New York: Academic Press.

Bell, C. C. (2001). Memory-based expectations in electrosensory systems. *Curr. Opin. Neurobiol.* **11**, 481-487.

Bell, C. C., Han, V. Z., Sugawara, Y. and Grant, K. (1997). Synaptic plasticity in a cerebellum-like structure depends on temporal order. *Nature* **387**, 278-281.

Berman, N. J. and Maler, L. (1998a). Distal versus proximal inhibitory shaping of feedback excitation in the electrosensory lateral line lobe: implications for sensory filtering. *J. Neurophysiol.* **80**, 3214-3232.

Berman, N. J. and Maler, L. (1998b). Inhibition evoked from primary afferents in the electrosensory lateral line lobe of the weakly electric fish (*Apteronotus leptorhynchus*). *J. Neurophysiol.* **80**, 3173-3196.

Berman, N. J. and Maler, L. (1999). Neural architecture of the electrosensory lateral line lobe: adaptations for coincidence detection, a sensory searchlight and frequency-dependent adaptive filtering. *J. Exp. Biol.* **202**, 1243-1253.

Berman, N., Dunn, R. J. and Maler, L. (2001). Function of NMDA receptors and persistent sodium channels in a feedback pathway of the electrosensory system. *J. Neurophysiol.* **86**, 1612-1621.

Bodznick, D., Montgomery, J. C. and Carey, M. (1999). Adaptive mechanisms in the elasmobranch hindbrain. *J. Exp. Biol.* **202**, 1357-1364.

Chacron, M. J., Doiron, B., Maler, L., Longtin, A. and Bastian, J. (2003). Non-classical receptive field mediates switch in a sensory neuron's frequency tuning. *Nature* **423**, 77-81.

Chance, F. S., Nelson, S. B. and Abbott, L. F. (1998). Synaptic depression and the temporal response characteristics of V1 cells. *J. Neurosci.* **18**, 4785-4799.

Chance, F. S., Abbott, L. F. and Reyes, A. D. (2002). Gain modulation from background synaptic input. *Neuron* **35**, 773-782.

Cullen, K. E. (2004). Sensory signals during active versus passive movement. *Curr. Opin. Neurobiol.* **14**, 698-706.

Dayan, P. and Abbott, L. F. (2001). *Theoretical Neuroscience*. Cambridge, MA: MIT Press.

de la Rocha, J. and Parga, N. (2005). Short-term synaptic depression causes a non-monotonic response to correlated stimuli. *J. Neurosci.* **25**, 8416-8431.

Desai, N. S. and Walcott, E. C. (2006). Synaptic bombardment modulates muscarinic effects in forelimb motor cortex. *J. Neurosci.* **26**, 2215-2226.

Dittman, J. S., Kreitzer, A. C. and Regehr, W. G. (2000). Interplay between facilitation, depression, and residual calcium at three presynaptic terminals. *J. Neurosci.* **20**, 1374-1385.

Doiron, B., Longtin, A., Turner, R. W. and Maler, L. (2001). Model of gamma frequency burst discharge generated by conditional backpropagation. *J. Neurophysiol.* **86**, 1523-1545.

Doiron, B., Chacron, M. J., Maler, L., Longtin, A. and Bastian, J. (2003). Inhibitory feedback required for network oscillatory responses to communication but not prey stimuli. *Nature* **421**, 539-543.

Fellous, J. M., Rudolph, M., Destexhe, A. and Sejnowski, T. J. (2003). Synaptic background noise controls the input/output characteristics of single cells in an *in vitro* model of *in vivo* activity. *Neuroscience* **122**, 811-829.

Fortune, E. S. and Rose, G. J. (2003). Voltage-gated Na^+ channels enhance the temporal filtering properties of electrosensory neurons in the torus. *J. Neurophysiol.* **90**, 924-929.

Higley, M. J. and Contreras, D. (2006). Balanced excitation and inhibition determine spike timing during frequency adaptation. *J. Neurosci.* **26**, 448-457.

Kuhn, A., Aertsen, A. and Rotter, S. (2004). Neuronal integration of synaptic input in the fluctuation-driven regime. *J. Neurosci.* **24**, 2345-2356.

Lewis, J. E. and Maler, L. (2002). Dynamics of electrosensory feedback: short-term plasticity and inhibition in a parallel fiber pathway. *J. Neurophysiol.* **88**, 1695-1706.

Lewis, J. E. and Maler, L. (2004). Synaptic dynamics on different time scales in a parallel fiber feedback pathway of the weakly electric fish. *J. Neurophysiol.* **91**, 1064-1070.

Longtin, A., Doiron, B. and Bulsara, A. R. (2002). Noise-induced divisive gain control in neuron models. *Biosystems* **67**, 147-156.

Marder, E. (2006). Neurobiology: extending influence. *Nature* **441**, 702-703.

Mehaffey, W. H., Doiron, B., Maler, L. and Turner, R. W. (2005). Deterministic multiplicative gain control with active dendrites. *J. Neurosci.* **25**, 9968-9977.

Mikula, S. and Niebur, E. (2003). Synaptic depression leads to nonmonotonic frequency dependence in the coincidence detector. *Neural Comput.* **15**, 2339-2358.

Mittmann, W. and Hausser, M. (2007). Linking synaptic plasticity and spike output at excitatory and inhibitory synapses onto cerebellar Purkinje cells. *J. Neurosci.* **27**, 5559-5570.

Moller, P. (1995). *Electric Fishes: History and Behavior*. London: Chapman & Hall.

Nelson, M. E. and MacIver, M. A. (2006). Sensory acquisition in active sensing systems. *J. Comp. Physiol. A* **192**, 573-586.

Nelson, M. E. and Paulin, M. G. (1995). Neural simulations of adaptive reafference suppression in the elasmobranch electrosensory system. *J. Comp. Physiol. A* **177**, 723-736.

Nowotny, T., Szucs, A., Pinto, R. D. and Selverston, A. I. (2006). StdpC: a modern dynamic clamp. *J. Neurosci. Methods* **158**, 287-299.

Oswald, A. M., Chacron, M. J., Doiron, B., Bastian, J. and Maler, L. (2004). Parallel processing of sensory input by bursts and isolated spikes. *J. Neurosci.* **24**, 4351-4362.

Prinz, A. A., Abbott, L. F. and Marder, E. (2004). The dynamic clamp comes of age. *Trends Neurosci.* **27**, 218-224.

Rabbah, P. and Nadim, F. (2005). Synaptic dynamics do not determine proper phase of activity in a central pattern generator. *J. Neurosci.* **25**, 11269-11278.

Roberts, P. D. (2000). Modeling inhibitory plasticity in the electrosensory system of mormyrid electric fish. *J. Neurophysiol.* **84**, 2035-2047.

Sanger, T. D. (2003). Neural population codes. *Curr. Opin. Neurobiol.* **13**, 238-249.

Sas, E. and Maler, L. (1983). The nucleus praeeminentialis: a Golgi study of a feedback center in the electrosensory system of gymnotid fish. *J. Comp. Neurol.* **221**, 127-144.

Sas, E. and Maler, L. (1987). The organization of afferent input to the caudal lobe of the cerebellum of the gymnotid fish *Apteronotus leptorhynchus*. *Anat. Embryol.* **177**, 55-79.

Sharp, A. A., O'Neil, M. B., Abbott, L. F. and Marder, E. (1993). Dynamic clamp: computer-generated conductances in real neurons. *J. Neurophysiol.* **69**, 992-995.

Sorensen, M., DeWeerth, S., Cymbalyuk, G. and Calabrese, R. L. (2004). Using a hybrid neural system to reveal regulation of neuronal network activity by an intrinsic current. *J. Neurosci.* **24**, 5427-5438.

Tan, A. Y., Atencio, C. A., Polley, D. B., Merzenich, M. M. and Schreiner, C. E. (2007). Unbalanced synaptic inhibition can create intensity-tuned auditory cortex neurons. *Neuroscience* **146**, 449-462.

Wolfart, J., Debay, D., Le Masson, G., Destexhe, A. and Bal, T. (2005). Synaptic background activity controls spike transfer from thalamus to cortex. *Nat. Neurosci.* **8**, 1760-1767.

Wu, G. K., Li, P., Tao, H. W. and Zhang, L. I. (2006). Nonmonotonic synaptic excitation and imbalanced inhibition underlying cortical intensity tuning. *Neuron* **52**, 705-715.